Observations of diurnal and spatial variability of radiative forcing by equatorial deep convective clouds

Observations of diurnal and spatial variability of radiative forcing by equatorial deep convective clouds

Sophie M. J. Nowicki

Centre for Polar Observation and Modelling, Department of Space and Climate Physics, University College London, London, UK

Christopher J. Merchant

Atmospheric and Environmental Science, School of GeoSciences, University of Edinburgh, Edinburgh, UK

Received 23 September 2003; revised 9 December 2003; accepted 25 March 2004; published 9 June 2004.

[1] From geostationary satellite observations of equatorial Africa and the equatorial east Atlantic during May and June 2000 we explore the radiative forcing by deep convective cloud systems in these regions. Deep convective clouds (DCCs) are associated with a mean radiative forcing relative to non–deep convective areas of -39 W m^{-2} over the Atlantic Ocean and of +13 W m^{-2} over equatorial Africa ($\pm$10 W m^{-2} in both cases). We show that over land the timing of the daily cycle of convection relative to the daily cycle in solar illumination and surface temperature significantly affects the mean radiative forcing by DCCs. Displacement of the daily cycle of DCC coverage by 2 hours changes their overall radiative effect by $\sim$10 W m^{-2}, with implications for the simulation of the radiative balance in this region. The timing of the minimum DCC cover over land, close to noon local time, means that the mean radiative forcing is nearly maximized. *INDEX TERMS:* 3314 Meteorology and Atmospheric Dynamics: Convective processes; 3359 Meteorology and Atmospheric Dynamics: Radiative processes; 0360 Atmospheric Composition and Structure: Transmission and scattering of radiation; *KEYWORDS:* convection, radiative forcing, diurnal cycle

Citation: Nowicki, S. M. J., and C. J. Merchant (2004), Observations of diurnal and spatial variability of radiative forcing by equatorial deep convective clouds, *J. Geophys. Res.*, *109*, D11202, doi:10.1029/2003JD004176.

1. Introduction

[2] Cloud systems associated with equatorial deep convection strongly modify the outgoing irradiance spectrum at the top of the atmosphere. Because the albedo of optically thick clouds (0.6 or more) exceeds average values over ocean and land, the "shortwave" (SW, <4 μm) irradiance, comprising reflected solar radiation, is enhanced by up to $\sim$1000 W m^{-2}, depending on the solar zenith angle, cloud albedo, and underlying cloud-free albedo. The "longwave" (LW, >4 μm) irradiance, comprising thermally emitted radiation, is decreased by $\sim$100 W m^{-2} because the cloud top is at a temperature representative of the upper troposphere ($\sim$200 K).

[3] "Cloud forcing" is the change in net outgoing irradiance caused by the presence of the cloud. Radiation budget observations [*Ramanathan et al.*, 1989; *Harrison et al.*, 1990; *Cess et al.*, 2001] have indicated that average cloud forcing in convective areas is within $\sim$10 W m^{-2} of zero (especially over the maritime continent), such that the radiation balance at the top of the atmosphere is similar to that in adjacent nonconvective areas. By correlating Earth Radiation Budget Experiment cloud radiative forcing and International Satellite Cloud Climatology Project cloud type, *Kiehl* [1994] found that optically thick, high clouds determine the longwave and shortwave cloud forcing, and Kiehl suggested that the dominant factor in the cancellation is the height of the tropical tropopause. The work of *Cess et al.* [2001] indicates that it is the average of different cloud types ranging from optically thick convective clouds to thin cirrus clouds which gives rise to near-zero cloud forcing. It has been debated whether this degree of cancellation between the LW and SW effects implies the action of some feedback mechanism that drives the radiation balance of convective areas toward that of surrounding nonconvective areas. *Hartmann et al.* [2001] have proposed a heuristic model for such a feedback mechanism for oceanic deep convective regions and have pointed out the importance of global climate models being able to represent any such feedback.

[4] Here we investigate the extent to which the timing of deep convective activity relative to the diurnal cycles of illumination and surface temperature plays a role in determining the daily mean convective system radiative forcing. This is done in detail for an ocean and land region over a 2-month period, yielding one particular example of the role these diurnal cycles play in determining the overall forcing. Tropical convective systems with horizontal dimensions of 20–200 km have lifetimes of 6–18 hours, with larger systems able to survive a day or more [*Machado and Rossow*, 1993]. During the course of this lifetime the structure of the clouds of the convective system evolves with associated changes in albedo and mean cloud top

0148-0227/04/2003JD004176

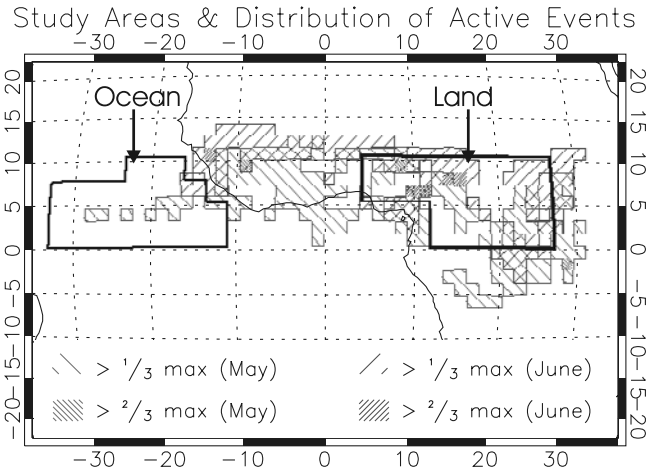

Figure 1. Map of the study area and definition of the ocean and land boxes. The distribution of active events in May and June 2000 is also shown, relative to the maximum number of events in any cell in each month (120 events for May, 92 events for June). See color version of this figure in the HTML.

temperature. Briefly, the formative convective system is dominated by very high albedo convective cloud over small areas; it develops a surrounding anvil cloud in its mature stage, with somewhat lower albedo, and it dissipates after convection ceases, breaking into anvil cloud fragments that become optically thinner with time. In order to explore how the daily cycle in deep convective cloud (DCC) characteristics interacts with the diurnal cycles of illumination and temperature to determine the overall cloud forcing from convective systems, we use satellite observations of sufficiently high temporal resolution to resolve these cycles in detail.

[5] We use full resolution data from Meteosat-7, a visible and infrared radiometer placed in geostationary orbit at 0°E, 0°N. The imagery has spatial resolutions of 2.5 km for the visible light spectrometer (VIS) (0.45–1 μm) and 5 km for the two infrared channels (a water vapor (WV) channel around 6.7 μm and a thermal infrared (IR) channel around 11.5 μm). The observations are made at half-hourly intervals, with the scanning time over the equator of the first slot of each day at roughly 0015 UTC. The area of our study is approximately from 37°W to 37°E and 22°S to 22°N and is shown in Figure 1. (Because we retain the satellite projection throughout, the latitude-longitude grid is curvilinear). The data span May and June 2000. This is a relatively short period from a single year, and in that sense the detailed results are of limited generality for the region. On the other hand, this has allowed us to perform the first fully time-resolved analysis, which demonstrates and quantifies the sensitivity of DCC forcing to the timing of the convective cycle within the day.

2. Irradiance Estimates From Meteosat-7

[6] Meteosat-7 does not directly observe the full-spectrum irradiances we require for this study, so these must be estimated. Raw digital counts are transformed to channel-integrated radiance using calibration coefficients provided by the satellite operators, EUMETSAT (available at http://www.eumetsat.de). The outgoing LW radiation (OLR) estimate is formed by the method of *Schmetz and Liu* [1988]. For Meteosat-7 the coefficients have been derived by M. Koenig (personal communication, 2002) using the Maryland Terrestrial Radiation Package (www.meto.umd.edu/~ezra/MDTERP.dir).

[7] The outgoing SW radiation (OSR) is estimated using the VIS radiance, L_{VIS}; thus

$$\mathrm{OSR} = \frac{\pi L_{\mathrm{VIS}} S_0}{A(\theta, \varphi, \theta_s) E_0},$$

where θ, φ, and θ_s are, respectively, the satellite zenith angle, solar zenith angle, and relative azimuth at the viewed point, S_0 is the solar "constant" (here, 1365 W m^{-2}), E_0 is the solar constant filtered according to the VIS channel response (693.2 W m^{-2}), and A is an anisotropic reflectance factor that modifies the ratio between radiance and irradiance according to the Sun surface satellite geometry and the surface type. The models of A were based on the works by *Saunders et al.* [1983] and *Suttles et al.* [1988], which specify five surface types (land, desert, ocean, land-ocean mix, and snow) and four levels of cloudiness (clear, partly cloudy, mostly cloudy, and overcast). To apply the appropriate anisotropic reflectance factor, we distinguished "ocean" from "land" by the geolocation of image pixels and "land" from "desert" by a threshold on monthly minimum albedo. The cloudiness level was assessed on the basis of albedo compared to monthly minimum albedo. (Note that only the anisotropy correction factor depends on the classification, the main determinant of the OSR estimate being the observed L_{VIS}.)

[8] Estimating irradiance from channel radiances is prone to systematic error related to the angular models and spectral extrapolations involved. To verify that our irradiance estimates are fit for our purpose, we have compared our OLR and OSR with independent radiation budget observations from the Clouds and Earth Radiant Energy System (CERES) program (version "ES9"). The CERES overpass is at 1030 local solar time (LST). Accounting for published CERES systematic error estimates, CERES random error, and error in time matching, the error for each CERES cell was estimated to be ±13 W m^{-2} for OSR and ±3 W m^{-2} for OLR. We took CERES "hourbox" data averaged over 2.5° cells and matched each observation with the OSR and OLR from the Meteosat-7 imagery to within a quarter of an hour (Figures 2a and 2b), there being typically two observations per day per cell. As well as the retrieval errors, there are effects of matching (such as movement of clouds within the time window), which may account for some extreme points in the individual matched observations. For the 49,878 matched observations the mean differences are −19 W m^{-2} for the OSR and 6 W m^{-2} for the OLR, while the standard deviations are 37 W m^{-2} and 15 W m^{-2}, respectively (and thus mean differences are highly significant statistically).

[9] In order to see whether there were any geographic systematic residuals, we derived monthly average irradi-

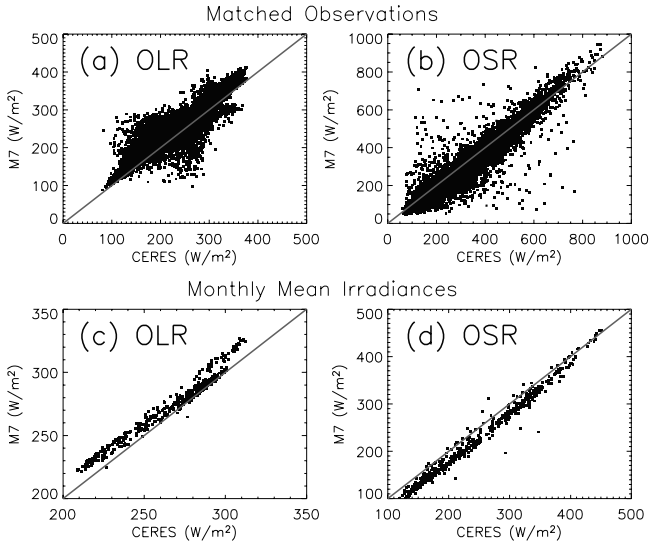

Figure 2. Individual matched CERES and Meteosat-7 observations for May and June 2000 for (a) OLR and (b) OSR. Monthly mean irradiances for (c) OLR and (d) OSR are also shown.

ances for each cell in the study area (Figures 2c and 2d). Compared to CERES, the Meteosat-7 OLR is smaller by 5% (i.e., by 10–15 W m^{-2}), with no systematic variation with OLR. Meteosat-7 OSR is 10% greater than CERES for low-albedo cells (OSR < 100 W m^{-2}) and is 5% greater than CERES with little systematic trend for higher-albedo cells (OSR > 100 W m^{-2}), i.e., is in the region of +10 W m^{-2} over the range of OSR. (In the daily mean this corresponds to roughly +4 W m^{-2}.) The difference map of the CERES and Meteosat-7 monthly mean irradiance (not presented) shows that there are no large systematic effects with location. Much of the analysis carried out in section 5 involves estimating radiation balance, which effectively involves a summation of these terms, so that these systematic differences tend to cancel; our daily Meteosat-7 radiation balance estimates therefore differ on average by about +8 W m^2 compared to the CERES calibration.

3. Identification and Classification of Deep Convective Clouds

[10] Previous investigators have used thresholds on the IR channel to identify deep convective clouds. *Machado et al.* [1998] identified convective systems in GOES data using thresholds of 245 and 218 K: cloud tops with temperatures <245 K corresponded to cloud top heights greater than 8–9 km, while the 218 K threshold identified the active convective cell because that temperature corresponds to top height between 12 and 13 km. *Mathon and Laurent* [2001] tracked Sahelian mesoscale systems on Meteosat images with IR thresholds of 253 K (which they estimated was the highest temperature associated with convection), 233 K (because it lies in the range of most commonly used thresholds), and 213 K (as an indicator of very deep convection).

[11] Here we identify deep convective clouds from WV brightness temperatures. Only clouds with cloud tops at or near the tropopause are present in WV imagery. Moreover, the background temperature in the WV channel (between high clouds) is more uniform at cloud scales than in the IR (being representative of the middle to upper troposphere rather than the surface). All these factors allow greater discrimination of cirrus shield edges in the WV imagery, while thicker components of the deep convective clouds are detectable in much the same way.

[12] Our aim is to identify all cloud components associated with deep convection: cirrus ("CIR"), the thicker anvil (or transition) cloud ("TRA"), and the convectively active region ("ACT"). Joint inspection of VIS, IR, and WV imagery determined that WV brightness temperature thresholds of 210 and 225 K are appropriate to delineate ACT and TRA clouds, respectively; this, of course, is somewhat subjective but similar to the approaches of previous investigators. CIR is identified from a combination of a texture measure (local standard deviation >0.6 K) and a dynamic threshold (10 K colder than a background temperature determined by filtering out short spatial scales). Figure 3 shows an example classification and compares it to the classification of Mathon and Laurent. Compared to Mathon and Laurent's classification, our classification of the subscene is more sensitive to the cirrus shield edge, and only the most active components of the cloud system are identified as active.

[13] The distribution of active events during May and June 2000 is shown in Figure 1. These mostly occur in the Intertropical Convergence Zone and follow its migration. Maximum concentrations of active events occur over elevated regions such as the Cameroon Mountains (7°N, 12°E), or the Fouta Djalon (10°N, 10°W). High concentrations of convective events also occur in coastal regions such as the Nigeria and Guinea coasts and over the Congo Basin. These observations are all consistent with previous work. Regions with more than two thirds of the maximum event frequency have been associated with initiation and dissipation regions [*Mathon and Laurent*, 2001; *Hodges and Thorncroft*, 1997]. Since most systems are short-lived, initiation and dissipation generally occur in the same regions. *Hodges and Thorncroft* [1997] suggest that downstream orography could inhibit storm propagation and that dissipation over the ocean is associated with cold sea surface temperatures.

4. Diurnal Cycle of Deep Convection

[14] The diurnal cycle of deep convection has been widely studied to try to understand the triggering of convection and the observed differences between land and ocean. DCCs in tropical Africa occur more frequently over land than over nearby ocean. Small convective systems occur somewhat more frequently over land than ocean, the reverse being true of large systems [*Machado and Rossow*, 1993].

[15] Over land, convective clouds are mainly initiated in the early afternoon (between noon and 1500 LST). These clouds later grow or merge into larger clusters owing to intensification of convection, and the maximum cloud coverage (and convective activity) occurs in late afternoon (1600–1900 LST). As the convection weakens in the morning (between 0300 and 1200 LST), the clusters

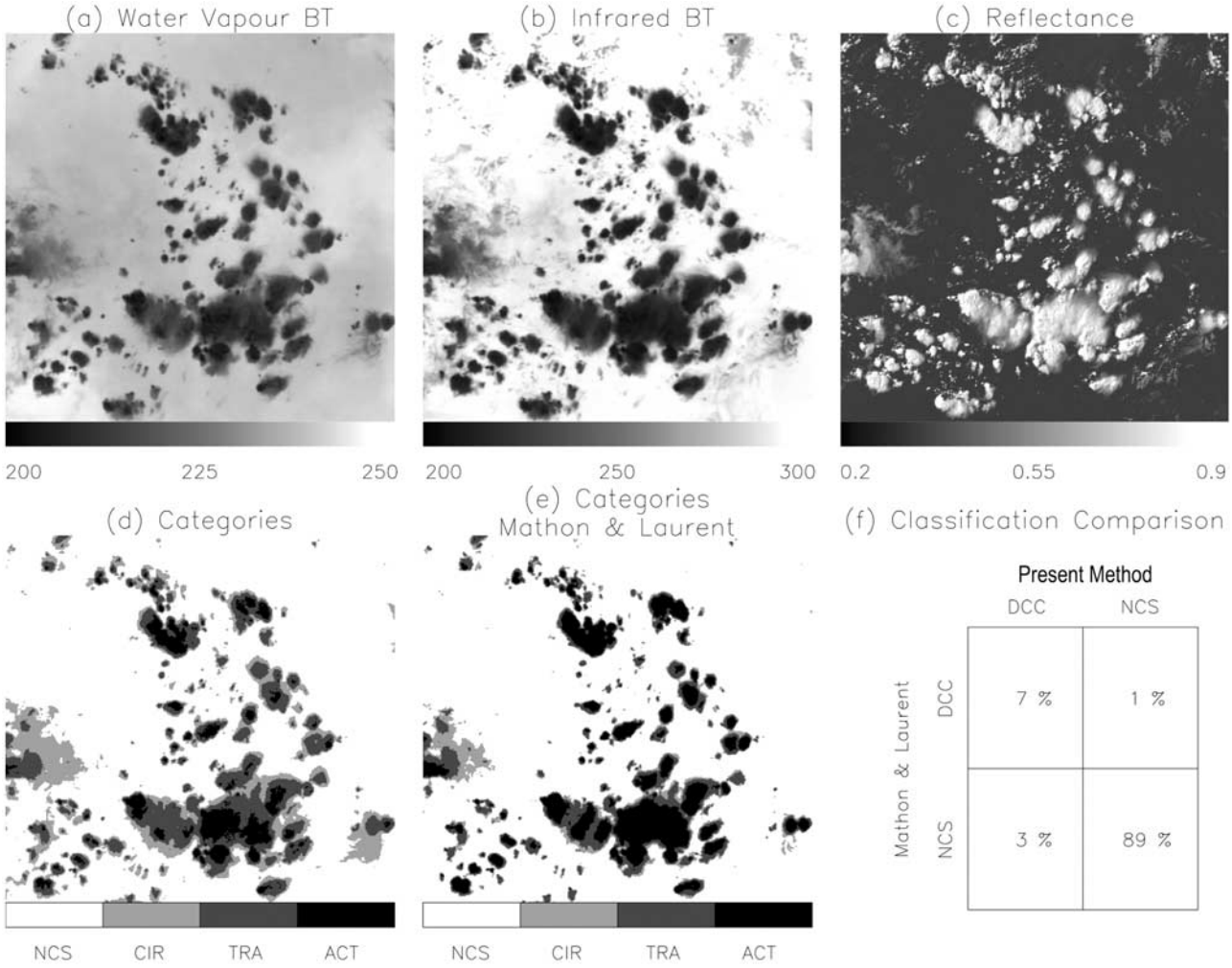

Figure 3. Classification of DCC cloud elements for a 1915 × 1915 km subscene. Shown are the following: (a) water vapor (WV) image; (b) infrared (IR) image; (c) visible light spectrometer (VIS) image; (d) classification into nonconvective (NCS), cirrus (CIR), transition (TRA), and active (ACT); (e) classification following Mathon and Laurent's method; and (f) percentages of pixels classified as DCC and NCS by our method and that of Mathon and Laurent, based on all pixels during May and June 2000. See color version of this figure in the HTML.

dissipate or split into smaller systems [*Machado and Rossow*, 1993; *Mathon and Laurent*, 2001]. In the course of the day the lower-tropospheric temperature (and moisture) increases owing to warming of the surface, thereby increasing convective instability and promoting the onset of convection. At nighttime, convection is suppressed because the radiative cooling of land enhances stability in the atmosphere.

[16] The data analyzed at full temporal and spatial resolution in this study are consistent with this general picture. We show in Figure 4a the daily cycle of DCC elements over the land subregion defined in Figure 1. We find the maximum prevalence of ACT to be around 1800 LST, while the maxima of the transition and cirrus coverage lag by 0.5 and 2.5 hours, respectively. The minima of DCC components are between 1100 and 1200 LST.

[17] The diurnal variation (Figure 4b) in the ocean subregion (defined in Figure 1) is less pronounced, with a shallow minimum in the active convective component around 1600 LST and a broad maximum in the early morning (in agreement with *Yang and Slingo* [2001]). However, in our study area the maximum cloud cover

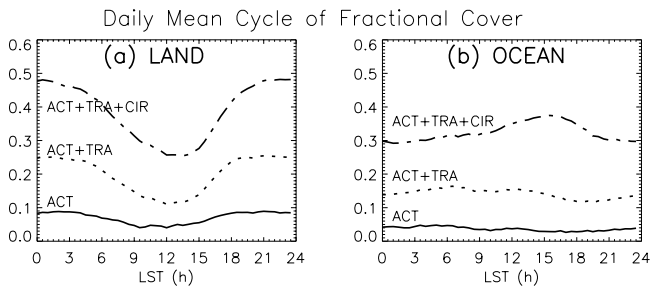

Figure 4. Diurnal cycle of clouds associated with deep convection over (a) land and (b) ocean subregion. Data are averaged over May and June 2000.

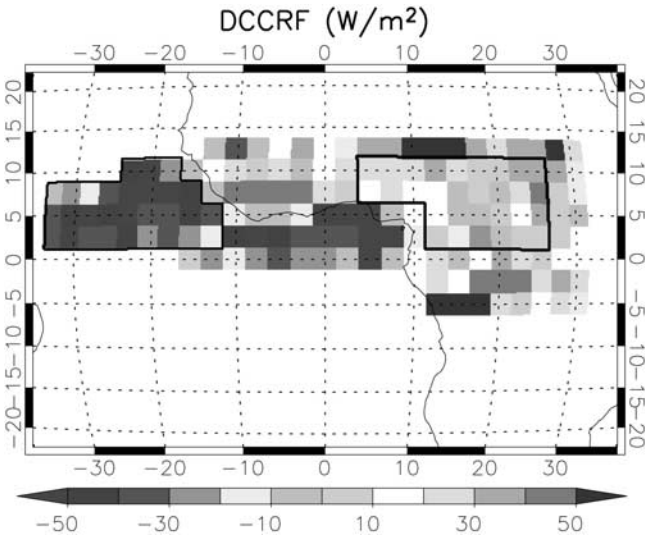

Figure 5. Time-mean deep convective cloud radiative forcing for May and June 2000. See color version of this figure in the HTML.

occurs in the middle afternoon (1500–1600 LST) and is associated with cirrus.

5. Deep Convective Cloud Radiative Forcing

[18] The deep convective cloud radiative forcing (DCCRF) which we calculate is a measure of the impact of DCCs on the Earth radiation balance and represents the change in net radiation associated with these cloud systems only. We have estimated DCCRF for each time slot by taking the difference of the radiation balance between DCCs and the remaining areas that are not convective systems (NCS) within 2.5° latitude-longitude cells. Although Africa has tremendous variations in surface albedo, in a 2.5° cell these variations are small (local standard deviation <0.03). The location of DCCs within a cell does not therefore bias the calculation of the DCCRF significantly. The cell size is as small as possible without there being a significant incidence of cells filled with DCC, for which no DCCRF can be calculated. There is an approximation in this method in that the presence of the DCC is assumed not to significantly change the radiation balance in the nearby NCS.

[19] Figure 5 shows the time-mean DCCRF for May and June for the cells where there were sufficient DCCs to make the estimate. DCCs over the ocean regions are seen to have a climate-cooling effect (since the DCCRF is negative), whereas they have a warming effect over land. The mean DCCRF for the ocean subregion is -39 W m^{-2}, and for the land subregion it is $+13$ W m^{-2}. Given the estimated error of ± 10 W m^{-2}, the ocean DCCRF is significantly negative, and the two regions are significantly different in this respect. The contrast in DCCRF between land and sea arises mainly from the effect of the different underlying albedo of land and sea (see the OSR curves of Figure 6a) and is modulated to a small degree by the different diurnal cycles of surface temperature of land and sea and by the greater variability of the proportion of ACT cloud within DCC systems (see the OLR curves of Figure 6b and compare with Figure 4).

[20] Figure 7a shows the variation of instantaneous DCCRF with respect to LST over land and ocean subregions, obtained by area-weighted averaging of DCCRF over May and June. During daytime the instantaneous effect of the DCCs is, as expected, a negative radiative forcing. DCCs increase the OSR to a degree that depends on the cloud surface albedo contrast, as shown by the fact that the principal difference between the land and ocean curves in Figure 7a is nearly proportional to the daily cycle of illumination.

[21] During nighttime the instantaneous effect of DCCs is a positive radiative forcing. The controlling factors in the (relatively small) differences between the land and ocean curves at night are the contrast between the diurnal surface temperature cycles of land and ocean, a difference in the cloud top temperature, and the composition of DCCs. For example, the early evening maximum in land DCCRF arises from the lower OLR of the DCCs indicating that their mean cloud top temperature is generally colder at that time, which is consistent with the maximum fractional coverage by ACT during the same time period (Figure 4).

[22] Diurnal variations in the coverage of the DCC components affect the (overall mean) DCCRF, more so for the land subregion, given the stronger daily cycle of DCC cover. We investigate the sensitivity of the DCCRF to

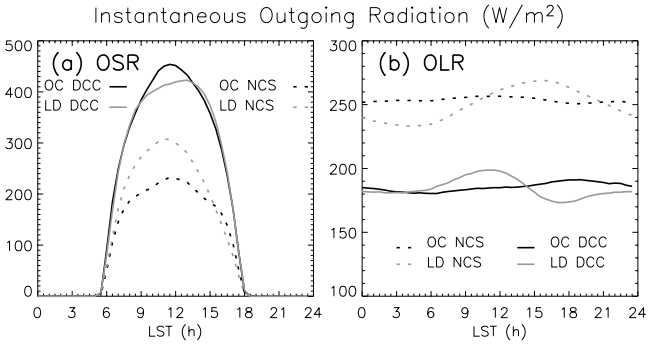

Figure 6. Mean instantaneous (a) OSR and (b) OLR for DCC and NCS over the land (LD) and ocean (OC) subregions for May and June 2000. See color version of this figure in the HTML.

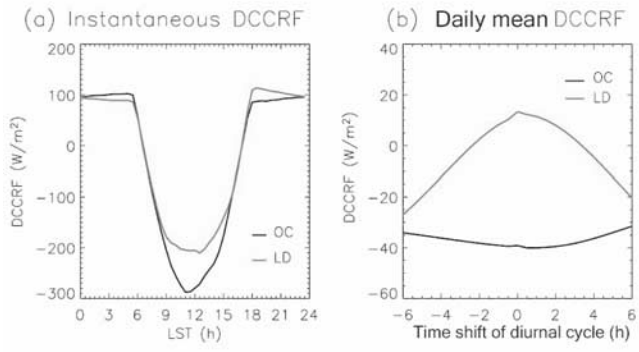

Figure 7. (a) Mean instantaneous DCCRF over the land and ocean subregions for May and June 2000 and (b) daily mean DCCRF as a function of the timing of the cycle of DCC cover. See color version of this figure in the HTML.

the timing of the cycle of DCC cover as follows. It is assumed that for each cloud component (ACT, TRA, and CIR) the instantaneous radiative forcing depends only on the LST. The instantaneous DCCRF is therefore a function of LST and of the relative prevalences of ACT, TRA, and CIR. The daily mean DCCRF is the weighted average of the instantaneous DCCRF, where the weighting is the DCC coverage at each time. We explore the effect of offsetting in local time the cycles of DCC coverage. For a given offset, synthetic values for the instantaneous DCCRF for each LST are generated using the prevalence of ACT, TRA, and CIR from an offset cycle. The average weighted by the (offset) DCC coverage then gives the time-mean DCCRF that would be obtained were the timing of the diurnal cycle different. The result is shown in Figure 7b.

[23] For the land subregion the timing of the DCC diurnal cycle affects the DCCRF such that, were the cycle either a few hours earlier or later, the DCCRF would shift in the direction of negative forcing by $\sim$10 W m^{-2}. With the timing of the DCC diurnal cycle that is actually observed, the DCCRF is nearly maximized over the land subregion (and minimized over the ocean subregion). This reflects the fact that the minimum of DCC coverage occurs at or just before noon over the land region. A given cloud cover has the greatest effect on OSR at noon when the solar irradiance scattered is a maximum. Since shifting the DCC diurnal cycle by more than 1 or 2 hours in either direction increases the DCC coverage at the time of peak insolation, the effect is in both cases to increase the overall OSR and therefore decrease the DCCRF. The sensitivity of DCCRF over the ocean subregion to the timing of the DCC diurnal cycle is much less.

6. Conclusions

[24] Using satellite observations of high space and time resolution for May and June 2000, we have shown that deep convective clouds over equatorial Africa and the equatorial east Atlantic caused a mean radiative forcing of +13 W m^2 and $-$39 W m^{-2}, respectively (errors are $\pm$10 W m^2). Thus the changes by these clouds to the longwave and shortwave radiation streams at the top of the atmosphere have a net effect that is not radiatively neutral. The ocean-land contrast in radiative forcing arises largely from the difference in underlying albedo, with a smaller contribution from differences in the composition of the clouds.

[25] While the mean radiative forcing of the deep convective systems is a few tens of watts per square meter, the instantaneous value varies diurnally between 100 and $-$300 W m^{-2} over ocean and between 120 and $-$200 W m^{-2} over land. Particularly over land, there is a diurnal cycle in convection (in both the fractional area covered and the relative areas of cloud components) whose timing is important in determining the mean radiative forcing. It is recognized that the phase of the diurnal cycle in convective activity is often poorly represented in general circulation models [e.g., *Yang and Slingo*, 2001]. For the land region studied here, the timing of the cycle of deep convection over land is such as to maximize the associated radiative forcing. To represent the mean radiative effect of these clouds to within $\pm$10 W m^{-2} in any model, the timing of the convection cycle needs to be correct to within $\sim$2 hours.

[26] **Acknowledgments.** In connection with the anisotropy models used, we wish to thank the Distributed Active Archive Center (Code 902) at the Goddard Space Flight Center, Greenbelt, Maryland, for putting these data in their present format and distributing them. The CERES Terra FM1 Edition1 ES9 data were obtained from the Atmospheric Sciences Data Center at NASA Langley Research Center. The Meteosat-7 imagery was provided by EUMETSAT, and we wish to thank M. Koenig of EUMETSAT for the coefficients used for OLR retrieval.

References

Cess, R. D., M. Zhan, B. A. Wielicki, D. F. Young, X. L. Zhou, and Y. Nikitenko (2001), The influence of the 1998 El Niño upon cloud-radiative forcing over the Pacific warm pool, *J. Clim.*, *14*, 2129–2137.

Harrison, E. F., P. Minnis, B. R. Barkstrom, V. Ramanathan, R. D. Cess, and G. G. Gibson (1990), Seasonal variation of cloud radiative forcing derived from the Earth Radiation Budget Experiment, *J. Geophys. Res.*, *95*(D11), 18,687–18,703.

Hartmann, D. L., L. A. Moy, and Q. Fu (2001), Tropical convection and the energy balance at the top of the atmosphere, *J. Clim.*, *14*, 4495–4511.

Hodges, K. I., and C. D. Thorncroft (1997), Distribution and statistics of African mesoscale convective weather systems based on the ISCCP Meteosat imagery, *Mon. Weather Rev.*, *125*, 2821–2837.

Kiehl, J. T. (1994), On the observed near cancellation between longwave and shortwave cloud forcing in the tropical regions, *J. Clim.*, *7*, 559–565.

Machado, L. A. T., and R. Rossow (1993), Structural characteristics and radiative properties of tropical cloud clusters, *Mon. Weather Rev.*, *23*, 3234–3260.

Machado, L. A. T., W. B. Rossow, R. L. Guedes, and A. W. Walker (1998), Life cycle variations of mesoscale convective systems over the Americas, *Mon. Weather Rev.*, *126*, 1630–1654.

Mathon, V., and H. Laurent (2001), Life cycle of Sahelian mesoscale convective cloud system, *Q. J. R. Meteorol. Soc.*, *127*, 377–406.

Ramanathan, V., R. D. Cess, E. F. Harrison, P. Minnis, B. R. Barkstrom, E. Ahmad, and D. Hartmann (1989), Cloud-radiative forcing and climate: Results from the Earth radiation budget experiment, *Science*, *243*, 57–63.

Saunders, R. W., L. L. Stowe, G. E. Hunt, and C. F. England (1983), An intercomparison between radiation budget estimates and METEOSAT 1, Nimbus 7 and TIROS-N satellites, *J. Clim. Appl. Meteorol.*, *22*, 546–559.

Schmetz, J., and Q. Liu (1988), Outgoing longwave radiation and its diurnal variation at regional scales derived from Meteosat, *J. Geophys. Res.*, *93*(D9), 1192–1204.

Suttles, J. T., R. N. Green, P. Minnis, G. L. Smith, W. F. Staylor, B. A. Weilicki, I. J. Walker, D. F. Young, V. R. Taylor, and L. L. Stowe (1988), Angular radiation models for Earth-atmosphere system, *NASA Ref. Publ.*, *1184*.

Yang, G. Y., and J. Slingo (2001), The diurnal cycle in the tropics, *Mon. Weather Rev.*, *129*, 784–801.

C. J. Merchant, Atmospheric and Environmental Science, School of GeoSciences, University of Edinburgh, James Clerk Maxwell Building, The King's Buildings, Mayfield Road, Edinburgh EH9 3JZ, UK. (c.merchant@ed.ac.uk)

S. M. J. Nowicki, Centre for Polar Observation and Modelling, Department of Space and Climate Physics, University College London, Pearson Building, Gower St., London WC1E 6BT, UK. (smn@cpom.ucl.ac.uk)